

A Tumor-Microenvironment-Responsive Lanthanide–Cyanine FRET Sensor for NIR-II Luminescence-Lifetime In Situ Imaging of Hepatocellular Carcinoma

Mengyao Zhao, Benhao Li, Yifan Wu, Haisheng He, Xinyan Zhu, Hongxin Zhang, Chaoran Dou, Lishuai Feng, Yong Fan, and Fan Zhang*

Deep tissue imaging in the second near-infrared (NIR-II) window holds great promise for widespread fundamental research. However, inhomogeneous signal attenuation due to tissue absorption and scattering hampers its application for accurate in vivo biosensing. Here, lifetime-based in situ hepatocellular carcinoma (HCC) detection in NIR-II region is presented using a tumor-microenvironment (peroxynitrite, ONOO⁻)-responsive lanthanide–cyanine Förster resonance energy transfer (FRET) nanosensor. A specially designed ONOO⁻-responsive NIR-II dye, MY-1057, is synthesized as the FRET acceptor. Robust lifetime sensing is demonstrated to be independent of tissue penetration depth. Tumor lesions are accurately distinguished from normal tissue due to the recovery lifetime. Magnetic resonance imaging and liver dissection results illustrate the reliability of lifetime-based detection in single and multiple HCC models. Moreover, the ONOO⁻ amount can be calculated according to the standard curve.

Biomedical luminescence imaging has shown significant potential for real-time investigations of live biological and physiological processes due to the advantages of fast feedback and high sensitivity.^[1–3] Over the past years, significant efforts have been made to produce fluorescent probes operating in the second near-infrared (NIR-II) window (1000–1700 nm), which offers enhanced penetration into biological tissues compared with visible to traditional first near-infrared window regions (700–1000 nm).^[4–18] However, accurate detection in deep tissue is hampered by the fact that luminescence signal intensity exhibits unavoidable and inhomogeneous attenuation caused by tissue absorption and scattering.^[6,19] Recently, luminescence lifetime imaging has been demonstrated to exhibit stable

lifetime value under bio-tissue using time-domain technique.^[19–22] However, realizing quantitative luminescence-lifetime in situ sensing for endogenous ions, protein interaction, tumor hypoxia, acute inflammation, and the tumor microenvironment still faces big challenges and is in urgent demand.

To address this challenge, we have turned to the NIR-II lifetime Förster resonance energy transfer (FRET) systems design. Since lanthanide nanoparticles show unique advantages including: 1) finely tunable excitation and emission wavelengths changing varied dopants,^[23–29] 2) long and adjustable lifetime from microseconds to milliseconds,^[19,20,30] and 3) stable luminescence property in physiological environment,^[23,31–34] they can be used as the

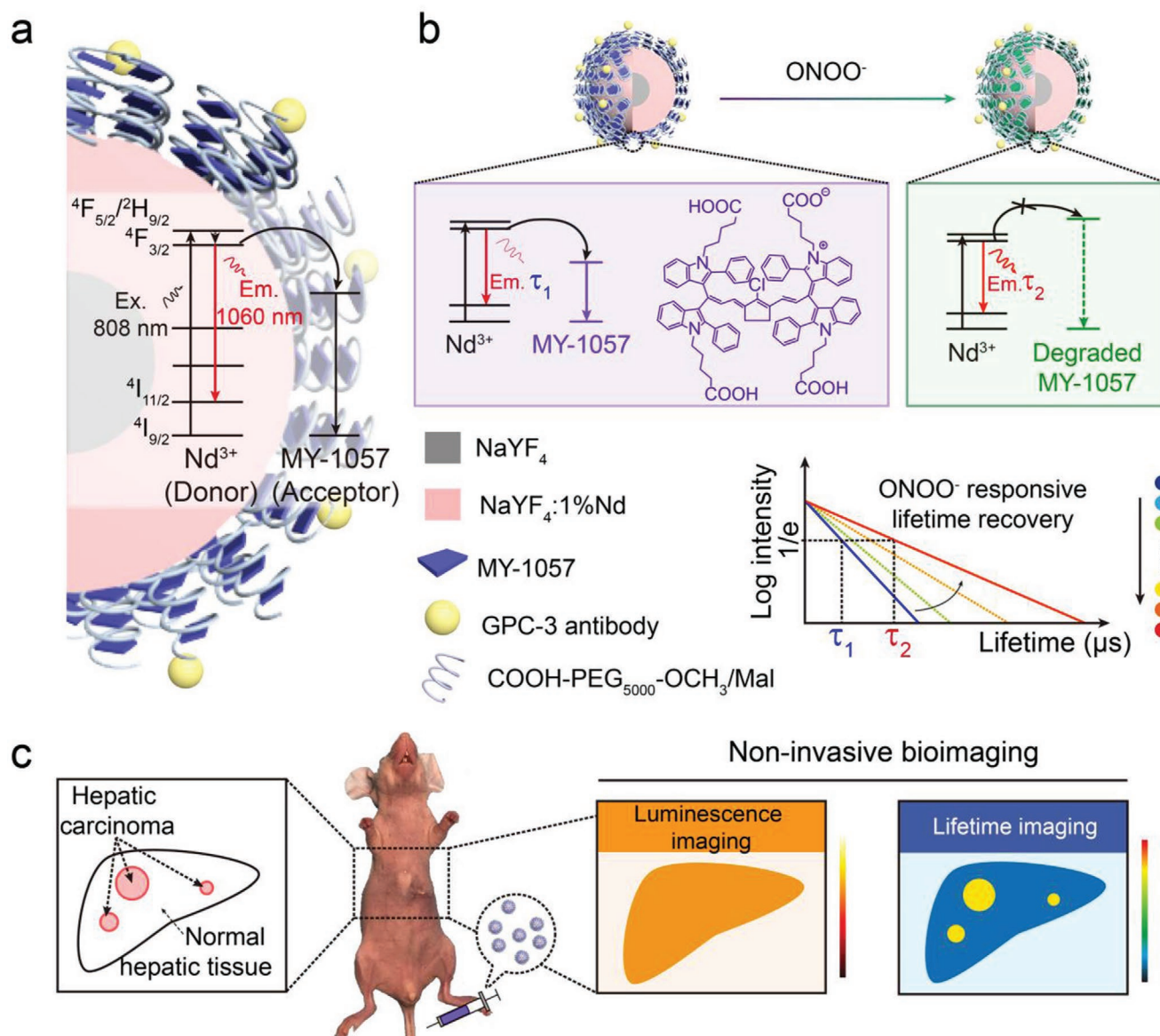
FRET donor.^[35–39] If the analyte sensitive energy acceptor can be obtained, this lifetime FRET sensor can be used for quantitative in vivo detection. Up to now, several contributions have been made based on tumor microenvironment^[40] (pH,^[41–43] reactive oxygen/nitrogen species,^[37,44] adenosine triphosphate,^[45] and enzymes^[46–48]) responsive luminescence probes. Among them, peroxynitrite (ONOO⁻) as a kind of reactive nitrogen species (RNS), is closely related to the nitration of proteins and receptors on immune cells in tumor microenvironment, which significantly influences the immunosuppression of tumor.^[44,49] Thus, through in situ detection of ONOO⁻, tumor lesions could be distinguished from normal tissue.^[50]

Herein, we report the NIR-II lifetime FRET sensor for hepatocellular carcinoma (HCC) detection based on a specially designed NIR-II cyanine dye, MY-1057, which is responsive to ONOO⁻ in the tumor microenvironment. In vivo quantitative sensing challenges are successfully overcome by integrating the lanthanide donor (Nd³⁺-doped nanoparticle) and the MY-1057 acceptor (Scheme 1a). The luminescence lifetime of the nanosensor can be decreased and determined by the amount of the surface modified acceptor. In response to RNS (especially ONOO⁻) at tumor lesions, the structure of energy acceptor MY-1057 degrades, leading to the lifetime recovery of the nanosensor (Scheme 1b). As a result, HCC lesions could be distinguished from normal hepatic tissue in lifetime imaging, while the intensity-based luminescence imaging fails to distinguish lesions due to the low signal-to-noise ratio caused

M. Zhao, Dr. B. Li, Y. Wu, Dr. H. He, X. Zhu, Dr. H. Zhang,
Prof. Y. Fan, Prof. F. Zhang
Department of Chemistry
Shanghai Key Laboratory of Molecular Catalysis and Innovative Materials
State Key Laboratory of Molecular Engineering of Polymers and iChem
Fudan University
Shanghai 200433, P. R. China
E-mail: zhang_fan@fudan.edu.cn
C. Dou, L. Feng
Shanghai Jiao Tong University Affiliated Sixth People's Hospital
Shanghai 200233, China

 The ORCID identification number(s) for the author(s) of this article can be found under <https://doi.org/10.1002/adma.202001172>.

DOI: 10.1002/adma.202001172



Scheme 1. Schematic illustration of lifetime-based detection of hepatocellular carcinoma (HCC) in the second near-infrared (NIR-II) window. a) Scheme of the ONOO⁻-responsive nanosensor DSNP@MY-1057-GPC-3. b) In the presence of ONOO⁻, the structure of the energy acceptor MY-1057 degrades sensitively, leading to the lifetime recovery in NIR-II region. c) Illustration of noninvasive NIR-II intensity- and lifetime-based imaging for HCC mice after administration of DSNP@MY-1057-GPC-3 nanosensor. HCC lesions could be distinguished from normal hepatic tissue from lifetime imaging, while the intensity-based luminescence imaging fails.

by the high accumulation of nanomaterials at liver (Scheme 1c). The lifetime results exhibit well correlation with clinical magnetic resonance imaging (MRI) results, illustrating the reliable detection of HCC by lifetime imaging. Furthermore, ONOO⁻ amount could be quantified in tumor lesions with various sizes.

To achieve both of the high luminescence intensity and stable lifetime for in vivo imaging, lanthanide downshifting nanoparticles (DSNPs) β -NaYF₄@NaYF₄:1%Nd were synthesized as NIR-II FRET donor with 1060 nm emission (Figure 1b and Figures S1–S3, Supporting Information). The core-shell nanostructures were further modified with 6-aminohexanoic acid and poly(ethylene glycol) acid (COOH-PEG₅₀₀₀-OCH₃ and COOH-PEG₅₀₀₀-Mal, 9:1) to enhance biocompatibility and

facilitate the incorporation of RNS-responsive dye MY-1057 into the particles via hydrophobic interaction (Scheme 1a and Figures S4–S6, Supporting Information). After MY-1057 encapsulation, DSNP@MY-1057 exhibited shortened luminescence lifetime from 305 ± 3 to 203 ± 2 μ s with FRET efficiency of 33% (Figure S7, Supporting Information). Furthermore, active targeting antibody glypican-3 (GPC-3) was conjugated with DSNP@MY-1057 to enhance the targeting ability at HCC lesion and finally form the DSNP@MY-1057-GPC-3 nanosensor with the hydrodynamic diameter of 52.4 nm (Scheme 1a and Figure 1a).

First in vitro RNS response capability of DSNP@MY-1057-GPC-3 nanosensor was evaluated. Upon ONOO⁻ treatment, MY-1057 absorption at 1057 nm gradually decreased

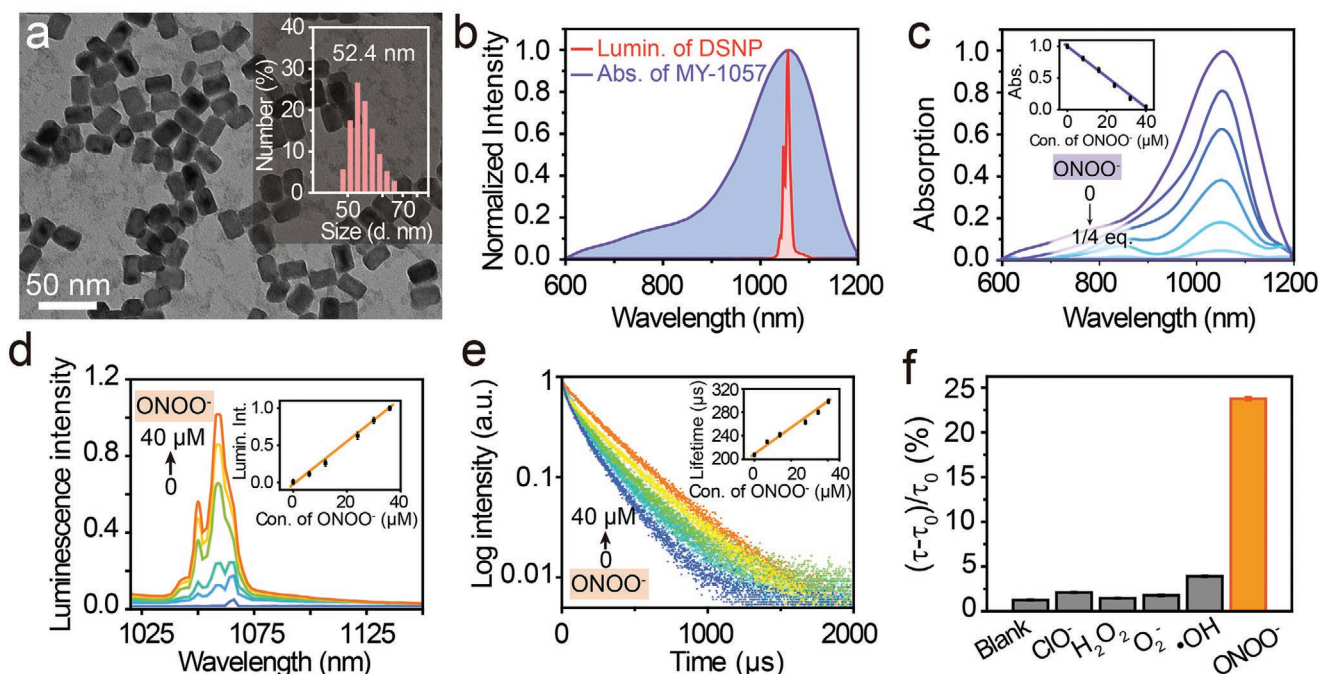


Figure 1. Characterization of luminescence-lifetime nanosensor and in vitro ONOO^- response. a) Transmission electron microscopy (TEM) images and dynamic light scattering (DLS) size distribution results of DSNP@MY-1057-GPC-3 nanoparticles. b) Overlap of the MY-1057 absorption and DSNP luminescence emission spectra. c) Absorption of MY-1057 as a function of ONOO^- (0–1/4 equiv.). d) Luminescence emission intensity and e) lifetime response of DSNP@MY-1057-GPC-3 at 1060 nm as a function ONOO^- concentration. f) Specificity of DSNP@MY-1057-GPC-3 for various radicals with lifetime changing at 1060 nm. ONOO^- : 40×10^{-6} M. ClO^- , H_2O_2 , O_2^- , $\cdot\text{OH}$: 200×10^{-6} M. τ_0 and τ represent for the luminescence lifetime of DSNP@MY-1057-GPC-3 at 1060 nm before and after responding to ONOO^- , respectively. Error bars, mean \pm s.d. ($n = 3$).

due to the structural degradation (Figure 1c), leading to the luminescence intensity recovery of DSNP@MY-1057-GPC-3 (Figure 1d and Figure S8, Supporting Information), along with lifetime recovery of the nanosensor from 203 ± 2 to 298 ± 2 μs (Figure 1e). Under 808 nm excitation, obvious lifetime recovery of DSNP@MY-1057-GPC-3 was only observed in the presence of ONOO^- , even the concentration of other radicals (ClO^- , H_2O_2 , O_2^- , and $\cdot\text{OH}$) were fivefold higher than that of ONOO^- , illustrating the high selectivity of ONOO^- detection (Figure 1f).

To obtain the optimal energy acceptor, series of dyes (denoted as MY-dyes) were designed with different terminal groups (Figure 2a). MY-dyes were synthesized from commercially available benzopyrrole derivatives through alkylated reaction and the Vilsmeier–Haack reaction (Figures S9–S12 and Tables S1–S3, Supporting Information). The absorption peaks of MY-dyes were located beyond 1000 nm and overlapped with the emission wavelength of DSNPs (Figure 2b and Figure S13, Supporting Information). However, only MY-1058 and MY-1057 were successfully encapsulated into the PEG layer on DSNPs surface (Figure 2c–e; Figures S14 and S15, Supporting Information), leading to obvious lifetime decreasing to 75 ± 1 and 203 ± 2 μs from 305 ± 3 μs , respectively. To investigate the encapsulating ability of MY-dyes, partition coefficient ($\log P$, a measure of hydrophobicity) of $\text{COOH-PEG}_{5000}\text{-OCH}_3$ and MY-dyes were measured (Table S4 and Figure S16, Supporting Information).^[51] $\log P$ of MY-1058 and MY-1057 were -1.10 ± 0.07 and 0.07 ± 0.02 , respectively, which were closer to $\text{COOH-PEG}_{5000}\text{-OCH}_3$ (-0.56 ± 0.04) compared to that of MY-1005 (0.51 ± 0.07). Next, the in vivo application potential was evaluated by measuring the

biostability of nanosensors. After adding fresh blood, lifetime of DSNP@MY-1057 remained stable while that of DSNP@MY-1058 changed from 75 ± 1 to 260 ± 2 μs immediately, which was due to the strong extraction effect of blood for MY-1058. Isothermal titration calorimetry was used to measure the binding ability between MY-1058 and several blood proteins including human serum albumin, bovine serum albumin, and bovine fibrinogen. MY-1058 tended to bind with bovine fibrinogen with binding parameter of $18\,140 \text{ L mol}^{-1}$ (Figure S17, Supporting Information), further demonstrating MY-1058 molecule can be extracted out of nanosensor in the presence of blood to induce the lifetime recovery. In addition, luminescence-lifetime stability of DSNP@MY-1057-GPC-3 was further investigated in various physical media including the whole blood, 10% fetal bovine serum, cell culture (Dulbecco's modified Eagle medium (DMEM)) and deionized water with pH 6. Nearly invariable lifetime value change was observed in 48 h (Figure S18, Supporting Information). Hence, due to the superior lifetime regulating range and good biostability, DSNP@MY-1057-GPC-3 was used as the optimal nanosensor for the following lifetime imaging experiment.

To investigate the reliability of lifetime-based DSNP@MY-1057-GPC-3 for ONOO^- sensing, intensity, and lifetime-based imaging of DSNP@MY-1057-GPC-3 were studied under different penetration depth by time-resolved NIR-II imaging system (Figure 3a). Before reacting with ONOO^- , DSNP@MY-1057-GPC-3 was filled in capillaries under phantom tissue (1% Intralipid) and bio-tissue, intensity-based imaging exhibited signal attenuation while lifetime-based imaging showed consistent lifetime values after penetrating through phantom

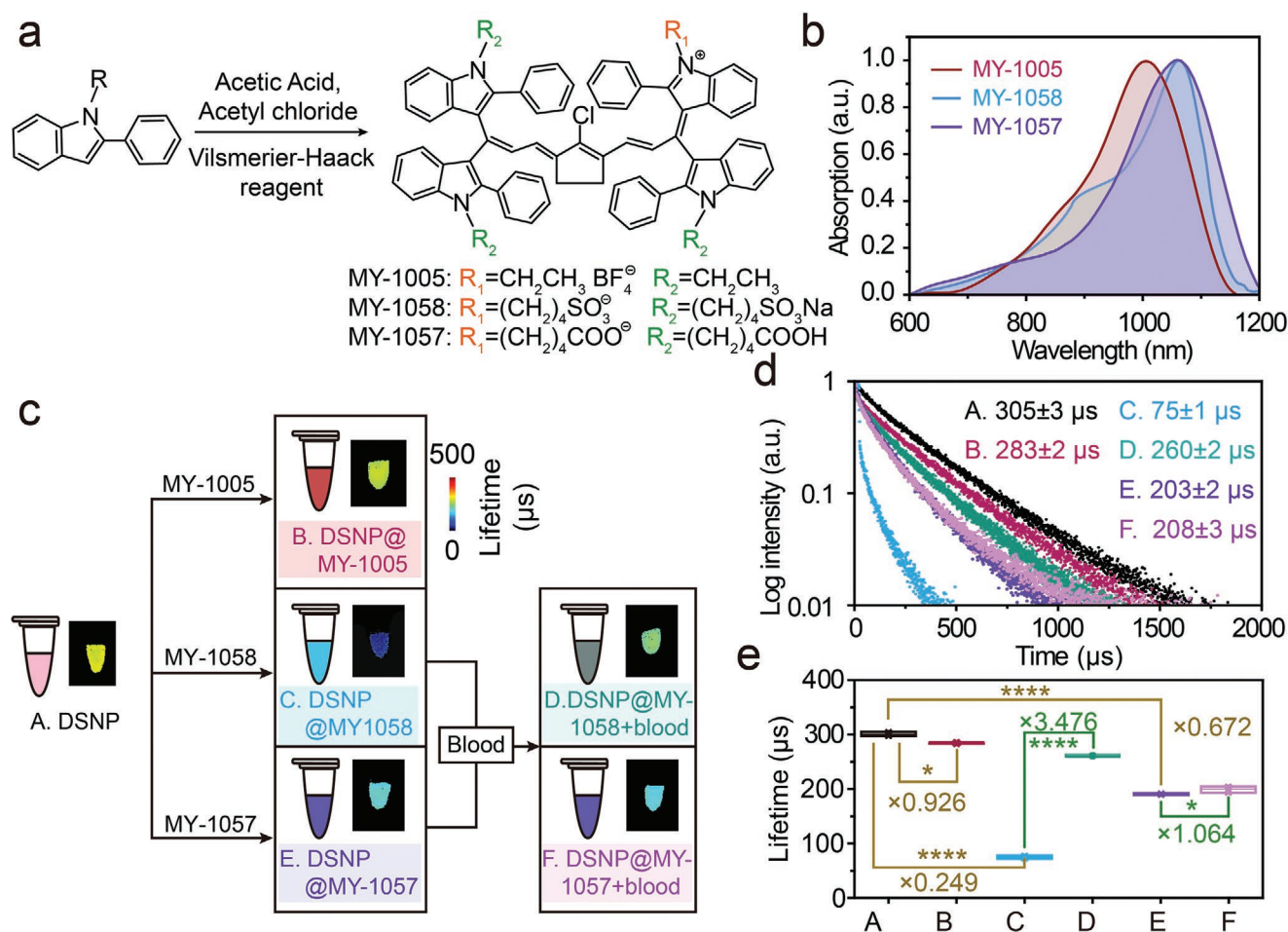


Figure 2. Optimizing energy acceptors by synthesizing MY series cyanine dyes for ONOO^- sensing. a) Synthesis of MY-dyes. b) Absorption spectra of MY-dyes in dimethyl sulfoxide (DMSO). c) Scheme illustration of optimization of energy acceptor. Insets: Luminescence lifetime images of samples A–F. d) Luminescence decay curves of samples A–F in (c). Lifetime values are indicated as mean \pm s.d. ($n = 3$). e) Lifetime values of DSNP and DSNP@MY-dyes before and after incubating with blood ($*0.01 < P < 0.05$, $****P < 0.0001$, numbers in (e) represent the relative multiple of lifetime changes for different samples).

tissue and bio-tissue (Figure S19, Supporting Information). In the presence of ONOO^- , NIR-II intensity-based imaging showed deep tissue penetration, and intensity signal of DSNP@MY-1057-GPC-3 raised linearly with increased ONOO^- concentration (Figure 3b). However, the slopes of intensity- ONOO^- functions were 900, 432, and 60 a.u. μM^{-1} under 0, 2, and 5 mm penetration depth, respectively (Figure 3e), illustrating that quantitative detection of ONOO^- using intensity-based imaging was not reliable due to signal attenuation caused by inhomogeneous scattering and absorption. In contrast, consistent lifetime response was obtained regardless of penetration depth (Figure 3c). In accord with lifetime spectral results (Figure 1e), lifetime recovered continuously from 202 ± 13 to $303 \pm 10 \mu\text{s}$ along with addition of ONOO^- (Figure 3c,d). More importantly, under phantom tissue with various penetration depth, lifetime values exhibited linearly correspondent to ONOO^- concentration and the lifetime- ONOO^- function slopes were almost identical ($3 \mu\text{s} \mu\text{M}^{-1}$ under 0, 2, and 5 mm penetration, Figure 3f). The stable slope value of lifetime- ONOO^- functions ensured the reliability of lifetime-based ONOO^- detection under bio-tissue (Figure 3g,h), and ONOO^- amount could be

calculated under unknown penetration depth according to the standard curve (Figure 3f and Equation (S1), Supporting Information). Furthermore, to investigate the distinguish ability of lifetime-based imaging, DSNP@MY-1057-GPC-3 nanosensors before and after responding to ONOO^- were encapsulated in poly(vinylpyrrolidone) (PVP) film to fabricate the short-lifetime background and long-lifetime targets. For lifetime-based imaging, long-lifetime targets with lifetime of 215 ± 9 and $224 \pm 9 \mu\text{s}$ were easily distinguished from short-lifetime background ($204 \pm 10 \mu\text{s}$), illustrating the capability of lifetime-based imaging for in vivo tumor detection (Figure S20, Supporting Information). Before in vivo imaging, the potential cytotoxicity of DSNP@MY-1057-GPC-3 was evaluated in human umbilical vein endothelial cells (HUVECs) and human hepatocellular carcinoma HepG-2 cells, which showed over 95% viability after incubation with $500 \mu\text{g mL}^{-1}$ nanosensor for 24 h, indicating the low cytotoxicity of DSNP@MY-1057-GPC-3 for both HUVEC and HepG-2 cells (Figure S21, Supporting Information).

The stable and reliable luminescence lifetime encouraged us to further explore its potential for in situ detection of HCC lesions. To build HCC model, human hepatocellular carcinoma

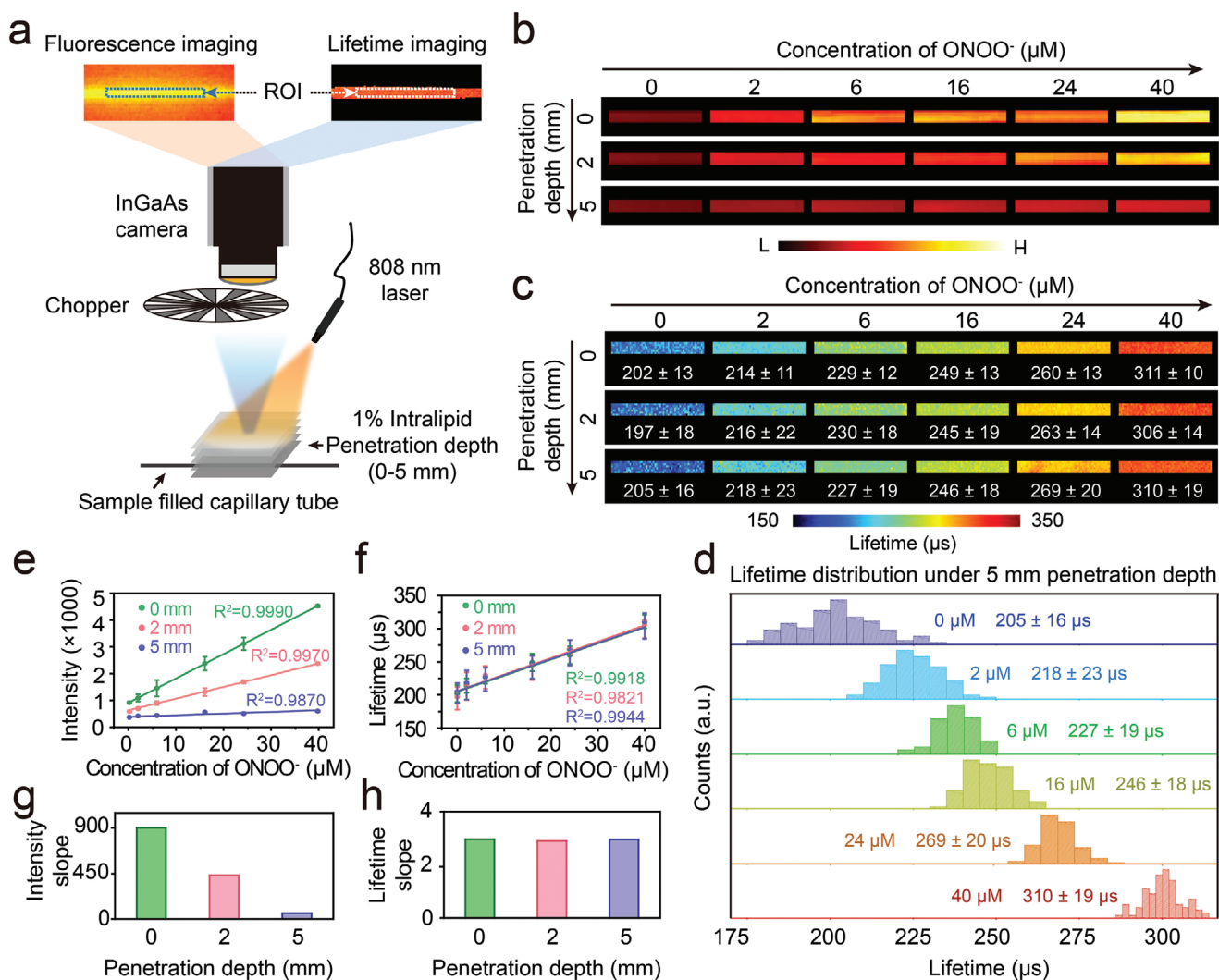


Figure 3. In vitro intensity- and lifetime-based imaging of DSNP@MY-1057-GPC-3 nanosensor in response to ONOO⁻ in NIR-II region. a) Experiment setup for intensity- and lifetime-based imaging of capillary under various penetration depth. Region of interest (ROI) during data processing was marked with blue and white dash box. b,e) Intensity- and c,f) lifetime-based imaging results as a function of ONOO⁻ concentration with DSNP@MY-1057-GPC-3 contained capillaries under different penetration depths. d) Lifetime distribution of DSNP@MY-1057-GPC-3 as a function of ONOO⁻ concentration under 5 mm penetration depth of 1% Intralipid. g,h) Slopes of functions extracted from (e) and (f). Error bars, mean ± s.d. (*n* = 3).

HepG-2 cells were injected into liver tissue of nude mice to mimic naturally occurring tumors. Then, the mice received DSNP@MY-1057-GPC-3 nanosensor by intravenous injection (15 mg kg⁻¹) (Figure 4a). The ≈50 nm hydrodynamic diameter led to efficient accumulation of nanosensors at liver with stable lifetime around 205 μs due to the reticuloendothelial system capture (Figure S22, Supporting Information). Tumor lesions could hardly be observed with NIR-II luminescence intensity imaging, while tumor lesions with lifetime from 212 ± 7 to 275 ± 49 μs were easily distinguished from normal hepatic tissue background (205 ± 7 μs) by lifetime-based imaging (Figure 4b,c). Tumor sizes and locations acquired from lifetime imaging exhibited excellent consistency with MRI and dissected liver white light results, suggesting the accuracy and reliability of lifetime imaging (Figure 4d and Figure S23, Supporting Information). Furthermore, to quantify the amount of ONOO⁻ at tumor lesions, nanosensor accumulation in tumors

was measured by inductively coupled plasma optical emission spectrometry, and the ONOO⁻ amount was calculated according to Equation (S1) in the Supporting Information. The amount of ONOO⁻ at tumor lesions raised with the increase of tumor volume (Figure 4e). Finally, HCC model with multiple lesions was established, three tumor lesions with lifetime from 215 ± 27 to 249 ± 43 μs were accurately distinguished from normal hepatic tissue with lifetime of 204 ± 10 μs (Figure 4f,g and Figure S24, Supporting Information). Moreover, lifetime imaging results for HCC with multiple lesions were well accord with MRI results and white light photo, further demonstrating the reliability of lifetime-based detection (Figure 4f). Hematoxylin–eosin (H&E) staining results showed negligible harm for organs including heart, liver, spleen, lung, and kidney at 24 h after DSNP@MY-1057-GPC-3 administration, indicating the low biotoxicity of DSNP@MY-1057-GPC-3 nanosensors (Figures S25 and S26, Supporting Information).

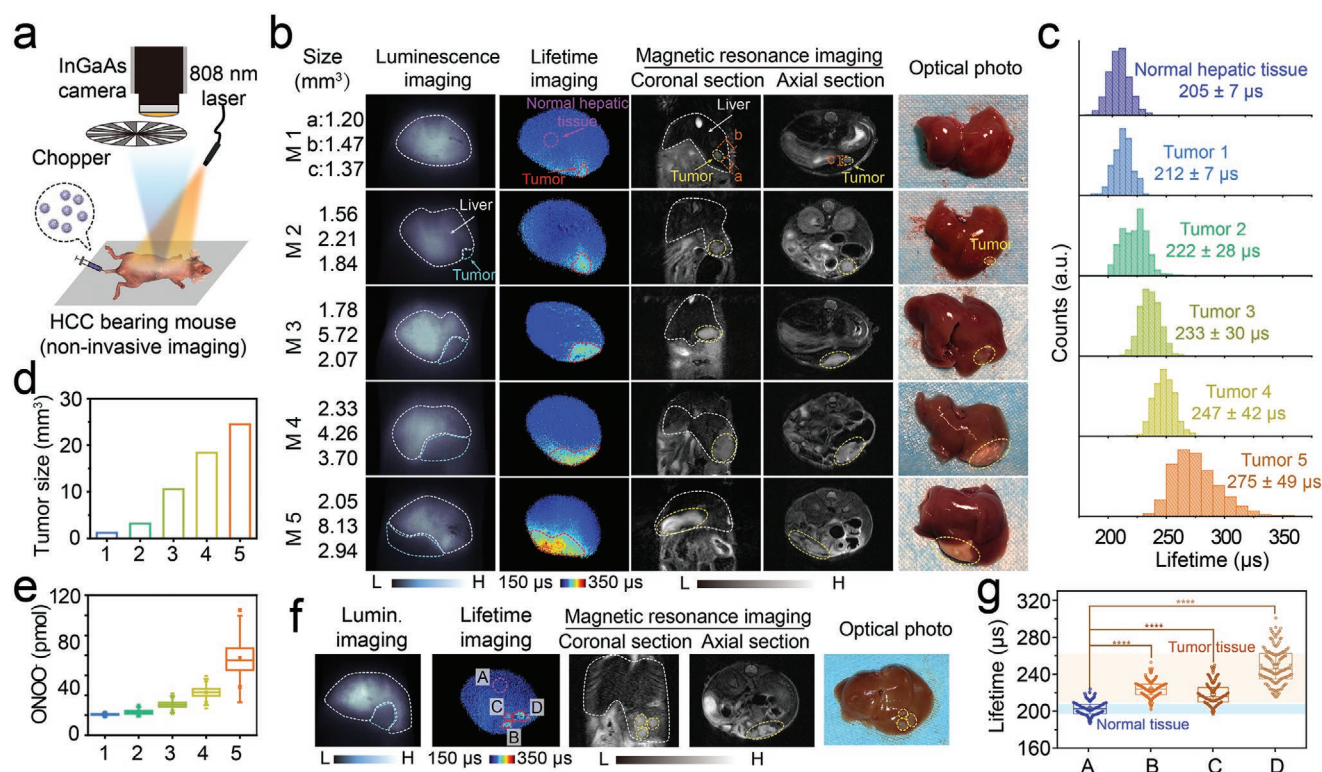


Figure 4. In situ HCC tumor detection by noninvasive NIR-II luminescence-lifetime imaging after administration of DSNP@MY-1057-GPC-3 nanosensor. a) Imaging setup for noninvasive lifetime imaging in NIR-II region. b) Noninvasive intensity-based imaging, lifetime-based imaging, and MRI of HCC-bearing mice and optical photo of dissected livers. Tumor lesions and normal hepatic tissues are marked as indicated. c) Luminescence lifetime distribution, d) measured size and e) calculated ONOO⁻ amount of Tumors 1–5. f) Noninvasive intensity-based imaging, lifetime-based imaging of a mouse bearing multiple HCC lesions and optical photo of the dissected liver. ROI A: normal hepatic tissue; ROI B–D: tumor lesions distinguished from lifetime imaging. g) Lifetime extracted from ROI A–D of (f).

In summary, an NIR-II lifetime-based ONOO⁻-responsive nanosensor was established using a lanthanide–cyanine FRET system. After administration in HCC-bearing mice, single or multiple lesions could be accurately distinguished from normal hepatic tissue by lifetime imaging due to the recovery lifetime responding to ONOO⁻ in the tumor microenvironment. Furthermore, the ONOO⁻ amount at tumor lesions could be quantitatively measured according to the in vitro standard curve. Additionally, lifetime imaging employs pulsed excitation and delayed detection, contributing to higher sensitivity and contrast by removing the autofluorescence background. The risk of thermal accumulation and damage to the tissue are also reduced compared to ordinary intensity imaging, rendering the use of high-power lasers less of a concern. Given lifetime measurement is immune to the constant background from ambient light, augmented reality can be integrated to enable a wide range of preclinical and clinical biomedical applications.

Experimental Section

For all the experiments, see the Supporting Information.

Supporting Information

Supporting Information is available from the Wiley Online Library or from the author.

Acknowledgements

M.Z. and B.L. contributed equally to this work. The work was supported by the National Key R&D Program of China (2017YFA0207303), National Natural Science Foundation of China (NSFC, 21725502 and 51961145403), and Key Basic Research Program of Science and Technology Commission of Shanghai Municipality (17JC1400100 and 19490713100). The authors appreciate Shiliang Tao and Jun He from Shanghai Chenguang Medical Technologies Co., Ltd. for the MRI measurement. The animal experiments were approved by the Shanghai Science and Technology Committee, and were carried out according to the guidelines of Fudan University's Administrative panel on Laboratory Animal Care. HUVECs and HepG-2 cells were provided by Stem Cell Bank, Chinese Academy of Science.

Conflict of Interest

The authors declare no conflict of interest.

Keywords

energy transfer, hepatocellular carcinoma detection, lanthanides, NIR-II dyes, NIR-II lifetime imaging

Received: February 19, 2020
Revised: May 3, 2020
Published online:

- [1] H. Kobayashi, M. Ogawa, R. Alford, P. L. Choyke, Y. Urano, *Chem. Rev.* **2010**, *110*, 2620.
- [2] J.-C. G. Bünzli, *Chem. Rev.* **2010**, *110*, 2729.
- [3] Y. Hori, S. Hirayama, M. Sato, K. Kikuchi, *Angew. Chem., Int. Ed.* **2015**, *54*, 14368.
- [4] J. Huang, J. Li, Y. Lyu, Q. Miao, K. Pu, *Nat. Mater.* **2019**, *18*, 1133.
- [5] S. Wang, Y. Fan, D. Li, C. Sun, Z. Lei, L. Lu, T. Wang, F. Zhang, *Nat. Commun.* **2019**, *10*, 1058.
- [6] G. Hong, A. L. Antaris, H. Dai, *Nat. Biomed. Eng.* **2017**, *1*, 0010.
- [7] B. Li, L. Lu, M. Zhao, Z. Lei, F. Zhang, *Angew. Chem., Int. Ed.* **2018**, *57*, 7483.
- [8] O. T. Bruns, T. S. Bischof, D. K. Harris, D. Franke, Y. Shi, L. Riedemann, A. Bartelt, F. B. Jaworski, J. A. Carr, C. J. Rowlands, M. W. B. Wilson, O. Chen, H. Wei, G. W. Hwang, D. M. Montana, I. Coropceanu, O. B. Achorn, J. Kloepper, J. Heeren, P. T. C. So, D. Fukumura, K. F. Jensen, R. K. Jain, M. G. Bawendi, *Nat. Biomed. Eng.* **2017**, *1*, 0056.
- [9] H. Wan, J. Yue, S. Zhu, T. Uno, X. Zhang, Q. Yang, K. Yu, G. Hong, J. Wang, L. Li, Z. Ma, H. Gao, Y. Zhong, J. Su, A. L. Antaris, Y. Xia, J. Luo, Y. Liang, H. Dai, *Nat. Commun.* **2018**, *9*, 1171.
- [10] C. Sun, B. Li, M. Zhao, S. Wang, Z. Lei, L. Lu, H. Zhang, L. Feng, C. Dou, D. Yin, H. Xu, Y. Cheng, F. Zhang, *J. Am. Chem. Soc.* **2019**, *141*, 19221.
- [11] R. Tian, Q. Zeng, S. Zhu, J. Lau, S. Chandra, R. Ertsey, K. S. Hettie, T. Teraphongphom, Z. Hu, G. Niu, D. O. Kiesewetter, H. Sun, X. Zhang, A. L. Antaris, B. R. Brooks, X. Chen, *Sci. Adv.* **2019**, *5*, eaaw0672.
- [12] J. Huang, C. Xie, X. Zhang, Y. Jiang, J. Li, Q. Fan, K. Pu, *Angew. Chem., Int. Ed.* **2019**, *58*, 15120.
- [13] A. L. Antaris, H. Chen, K. Cheng, Y. Sun, G. Hong, C. Qu, S. Diao, Z. Deng, X. Hu, B. Zhang, X. Zhang, O. K. Yaghi, Z. R. Alamparambil, X. Hong, Z. Cheng, H. Dai, *Nat. Mater.* **2016**, *15*, 235.
- [14] L. Bao, C. Liu, Z. Zhang, D. Pang, *Adv. Mater.* **2015**, *27*, 1663.
- [15] C. Li, W. Li, H. Liu, Y. Zhang, G. Chen, Z. Li, Q. Wang, *Angew. Chem., Int. Ed.* **2020**, *59*, 247.
- [16] Z. Zheng, D. Li, Z. Liu, H. Peng, H. Sung, R. T. K. Kwok, I. D. Williams, J. W. Y. Lam, J. Qian, B. Tang, *Adv. Mater.* **2019**, *31*, 1904799.
- [17] Kenry, Y. Duan, B. Liu, *Adv. Mater.* **2018**, *30*, 1870361.
- [18] J. Du, S. Liu, P. Zhang, H. Liu, Y. Li, W. He, C. Li, J. H. C. Chau, R. T. K. Kwok, J. W. Y. Lam, L. Cai, Y. Huang, W. Zhang, J. Hou, B. Tang, *ACS Appl. Mater. Interfaces* **2020**, *12*, 8040.
- [19] Y. Fan, P. Wang, Y. Lu, R. Wang, L. Zhou, X. Zheng, X. Li, J. A. Piper, F. Zhang, *Nat. Nanotechnol.* **2018**, *13*, 941.
- [20] Y. Lu, J. Zhao, R. Zhang, Y. Liu, D. Liu, E. M. Goldys, X. Yang, P. Xi, A. Sunna, J. Lu, Y. Shi, R. C. Leif, Y. Huo, J. Shen, J. A. Piper, J. P. Robinson, D. Jin, *Nat. Photonics* **2014**, *8*, 32.
- [21] D. H. Ortgies, M. Tan, E. C. Ximendes, B. del Rosal, J. Hu, L. Xu, X. Wang, E. Martin Rodriguez, C. Jacinto, N. Fernandez, G. Chen, D. Jaque, *ACS Nano* **2018**, *12*, 4362.
- [22] H. Sparks, H. Kondo, S. Hooper, I. Munro, G. Kennedy, C. Dunsby, P. French, E. Sahai, *Nat. Commun.* **2018**, *9*, 2662.
- [23] X. Song, S. Li, H. Guo, W. You, X. Shang, R. Li, D. Tu, W. Zheng, Z. Chen, H. Yang, X. Chen, *Angew. Chem., Int. Ed.* **2019**, *58*, 18981.
- [24] B. Zhou, B. Shi, D. Jin, X. Liu, *Nat. Nanotechnol.* **2015**, *10*, 924.
- [25] Z. Xue, S. Zeng, J. Hao, *Biomaterials* **2018**, *171*, 153.
- [26] S. Yan, X. Zeng, Y. Tang, B. Liu, Y. Wang, X. Liu, *Adv. Mater.* **2019**, *31*, 1905825.
- [27] Z. Yan, H. Qin, J. Ren, X. Qu, *Angew. Chem., Int. Ed.* **2018**, *57*, 11182.
- [28] B. Liu, C. Li, P. Yang, Z. Hou, J. Lin, *Adv. Mater.* **2017**, *29*, 1605434.
- [29] A. Yin, Y. Zhang, L. Sun, C. Yan, *Nanoscale* **2010**, *2*, 953.
- [30] M. Zhang, W. Zheng, Y. Liu, P. Huang, Z. Gong, J. Wei, Y. Gao, S. Zhou, X. Li, X. Chen, *Angew. Chem., Int. Ed.* **2019**, *58*, 9556.
- [31] S. Chen, A. Z. Weitemier, X. Zeng, L. He, X. Wang, Y. Tao, A. J. Y. Huang, Y. Hashimoto-dani, M. Kano, H. Iwasaki, L. K. Parajuli, S. Okabe, D. B. L. Teh, A. H. All, I. Tsutsui-Kimura, K. Tanaka, X. Liu, *Science* **2018**, *359*, 679.
- [32] P. Wang, Y. Fan, L. Lu, L. Liu, L. Fan, M. Zhao, Y. Xie, C. Xu, F. Zhang, *Nat. Commun.* **2018**, *9*, 2898.
- [33] Y. Zhong, Z. Ma, F. Wang, X. Wang, Y. Yang, Y. Liu, X. Zhao, J. Li, H. Du, M. Zhang, Q. Cui, S. Zhu, Q. Sun, H. Wan, Y. Tian, Q. Liu, W. Wang, K. C. Garcia, H. Dai, *Nat. Biotechnol.* **2019**, *37*, 1322.
- [34] M. Zhao, B. Li, P. Wang, L. Lu, Z. Zhang, L. Liu, S. Wang, D. Li, R. Wang, F. Zhang, *Adv. Mater.* **2018**, *30*, 1804982.
- [35] R. Deng, J. Wang, R. Chen, W. Huang, X. Liu, *J. Am. Chem. Soc.* **2016**, *138*, 15972.
- [36] M. Kong, Y. Gu, Y. Liu, Y. Shi, N. Wu, W. Feng, F. Li, *Small* **2019**, *15*, 1904487.
- [37] J. Peng, A. Samanta, X. Zeng, S. Han, L. Wang, D. Su, D. T. B. Loong, N. Y. Kang, S. J. Park, A. H. All, W. Jiang, L. Yuan, X. Liu, Y. T. Chang, *Angew. Chem., Int. Ed.* **2017**, *56*, 4165.
- [38] Y. I. Park, H. M. Kim, J. H. Kim, K. C. Moon, B. Yoo, K. T. Lee, N. Lee, Y. Choi, W. Park, D. Ling, K. Na, W. K. Moon, S. H. Choi, H. S. Park, S. Y. Yoon, Y. D. Suh, S. H. Lee, T. Hyeon, *Adv. Mater.* **2012**, *24*, 5755.
- [39] D. Zhang, L. Wang, X. Yuan, Y. Gong, H. Liu, J. Zhang, X. Zhang, Y. Liu, W. Tan, *Angew. Chem., Int. Ed.* **2020**, *59*, 695.
- [40] X. Hu, F. Li, S. Wang, F. Xia, D. Ling, *Adv. Healthcare Mater.* **2018**, *7*, 1800359.
- [41] Y. Wang, K. Zhou, G. Huang, C. Hensley, X. Huang, X. Ma, T. Zhao, B. D. Sumer, R. J. DeBerardinis, J. Gao, *Nat. Mater.* **2014**, *13*, 204.
- [42] F. Li, Y. Du, J. Liu, H. Sun, J. Wang, R. Li, D. Kim, T. Hyeon, D. Ling, *Adv. Mater.* **2018**, *30*, 1802808.
- [43] D. Ling, W. Park, S. J. Park, Y. Lu, K. S. Kim, M. J. Hackett, B. H. Kim, H. Yim, Y. S. Jeon, K. Na, T. Hyeon, *J. Am. Chem. Soc.* **2014**, *136*, 5647.
- [44] X. Ai, Z. Wang, H. Cheong, Y. Wang, R. Zhang, J. Lin, Y. Zheng, M. Gao, B. Xing, *Nat. Commun.* **2019**, *10*, 1087.
- [45] J. Tian, X. Zeng, X. Xie, S. Han, O. W. Liew, Y. T. Chen, L. Wang, X. Liu, *J. Am. Chem. Soc.* **2015**, *137*, 6550.
- [46] Y. Tang, Y. Li, X. Hu, H. Zhao, Y. Ji, L. Chen, W. Hu, W. Zhang, X. Li, X. Lu, W. Huang, Q. Fan, *Adv. Mater.* **2018**, *30*, 1801140.
- [47] Q. Wu, K. Y. Zhang, P. Dai, H. Zhu, Y. Wang, L. Song, L. Wang, S. Liu, Q. Zhao, W. Huang, *J. Am. Chem. Soc.* **2020**, *142*, 1057.
- [48] D. Ye, A. J. Shuhendler, L. Cui, L. Tong, S. S. Tee, G. Tikhomirov, D. W. Felsher, J. Rao, *Nat. Chem.* **2014**, *6*, 519.
- [49] C. Szabó, H. Ischiropoulos, R. Radi, *Nat. Rev. Drug Discovery* **2007**, *6*, 662.
- [50] J. Zhang, X. Zhen, P. K. Upputuri, M. Pramanik, P. Chen, K. Pu, *Adv. Mater.* **2017**, *29*, 1604764.
- [51] N. C. Tansil, Y. Li, C. P. Teng, S. Zhang, K. Y. Win, X. Chen, X. Y. Liu, M. Y. Han, *Adv. Mater.* **2011**, *23*, 1463.